Earth And Planetary Science Letters
August 2013, Volume 375 Pages 78-91
http://dx.doi.org/10.1016/j.epsl.2013.05.013
http://archimer.ifremer.fr/doc/00159/27031/

Sea-level change and free gas occurrence influencing a submarine landslide and pockmark formation and distribution in deepwater Nigeria

Riboulot Vincent [1, 2, *], Cattaneo Antonio [1], Sultan Nabil [1], Garziglia Sebastien [1], Ker Stephan [1], Imbert Patrice [3], Voisset Michel [1]

[1] IFREMER, Ctr Brest, Inst CARNOT EDROME, Brest, France.
[2] Univ Perpignan, F-66025 Perpignan, France.
[3] TOTAL, Pau, France.

* Corresponding author : tel.: +33 298 224257 ; fax: +33 298 224570 ;
email address : riboulot@ifremer.fr

Abstract :

A series of pockmarks observed at the seabed matches well the perimeter of a large submarine landslide, called NG1, located on the outer shelf and continental slope of the Eastern Gulf of Guinea. NG1 extends over 200 km2, is covered by a 120-m thick sedimentary layer which tapers downslope, and has an internal structure clearly identified in 3D seismic data consisting of three adjacent units on the upper continental slope. The pockmarks above NG1 have a diameter of several tens of meters and reveal distinct origins: (1) linked to >500 m deep fluid reservoirs, (2) rooted in NG1 internal discontinuities between NG1 units, and (3) well above NG1, superficially rooted in a regional conformity (D40), which marks the lowest sea level of the Marine Isotope Stage 6. The regional stratigraphic pattern of the study area is composed of muddy sedimentary sequences separated by correlative conformities and transgressive condensed units of coarser grain size. Mud-confined coarser-grained units constitute transient gas reservoirs favoring lateral gas migration and formation of pockmarks rooted in the condensed units. The buried NG1 landslide modifies the layered structure of the sedimentary column providing (1) overall, a barrier to fluid migration, and (2) localized pathways for fluid migration. The triggering factor for the formation of pockmarks above NG1 can be the variation of hydrostatic pressure driven by relative sea-level fall during Marine Isotopic Stages 6 and 2 and consequent gas exsolution and fluid flow. We anticipate our result to be a starting point for understanding the role of gas seeps on climate change worldwide. Furthermore, gas release intensifies during lowstands with relevant implication on global warming after ice ages.

Highlights

►This is the first study linking the effect of a landslide on gas migration pathways. ►Pockmark formation is reconstructed with geophysical and geotechnical data. ►The landslide occurred during a sea-level fall period. ►The timing of pockmark formation is in part controlled by 100-kyr eustatic cycles. ►Once buried, the landslide controls the spatial organization of pockmarks.

Keywords : pockmarks, fluid seepage, submarine landslide, sea-level changes, piezocone, Niger Delta

1. Introduction

Since the 1970s, studies of the ocean floor have revealed the presence of pockmarks on passive and active continental margins worldwide. Pockmarks are described as circular or near circular depressions, generally 10–200 m in diameter and some tens of meters in depth, but they may reach 1.5 km in diameter and 150 m in depth (Pilcher and Argent, 2007). When pockmarks are observed in vertical section (seismic profile), they are associated with a vertical chimney under the depression (Hustoft et al., 2007). In seismic sections, chimneys are characterized by either an interruption of seismic reflectors due to the gas charge (wipeout zone) (Hovland, 1983, Hovland, 1991 and Rao et al., 2001), or by an inflection of seismic reflectors (Hovland et al., 1984) corresponding to a velocity pull down effect or to a deformation of sedimentary layer where fluids migrate.

Since the first study about pockmarks (King and MacLean, 1970), where they were considered as randomly distributed features at the seafloor, their understanding has evolved. It is now widely accepted that pockmarks represent the morphological signature of fluid seepage (Hovland et al., 1984), where fluid may be biogenic and/or thermogenic gas (Rogers et al., 2006) or water (Harrington, 1985). During recent years, there has been much interest in the study of pockmarks because they represent potential pathways for important quantities of gas from sediments to the oceans (e.g. Vogt et al., 1999, Paull et al., 2002, Ussler et al., 2003, Dimitrov and Woodside, 2003, Hovland et al., 2002, Hovland et al., 2005 and Gay et al., 2006a).

The discovery of pockmark alignments has shown that their spatial organization may be the result of fluid seepage from underlying sedimentary structures such as fault systems, channels, mud volcanoes, mud diapirs, and glaciogenic deposits (e.g. Eichhubl et al., 2000; Pilcher and Argent, 2007; Forwick et al., 2009). The spatial distribution of pockmarks suggests that all the discontinuities affecting the sedimentary column represent potential drains for fluid flow, and that simple diffusion through the sediments cannot explain such structures (Abrams, 1992; Brown, 2000). Today it is recognized that pockmarks can be subdivided in two groups: non-random pockmarks, when their spatial distribution is related to identified buried geological features, and random pockmarks, when it is not (Pilcher and Argent, 2007).

The mechanisms behind pockmark formation are still poorly understood. Some hypotheses and conceptual models about pockmark formation have been proposed by various authors (eg. Josenhans et al., 1978; Hovland, 1987; Gay, 2002; Cartwright et al., 2007, Andresen et al., 2008, Cathles et al., 2010). Josenhans et al., (1978), Hovland (1987), and Gay (2002), for example, propose schematic models of pockmark formation involving gas pressure in a transient fluid reservoir, local sedimentation, and action of bottom currents, but are insufficient to have a comprehensive view of all factors governing fluid expulsion.

Many studies suggest the possible implication of mass transport complexes in pockmark development (Trincardi et al., 2004; Bayon et al., 2009; Plaza-Faverola et al., 2010; Sun et al., 2012), but the role of a landslide in the distribution and formation of pockmarks has never been the central subject of a study. The Eastern Niger Submarine Delta (ENSD; Fig. 1), situated in deepwater “Niger Delta”, deserves attention because: (1) there is significant evidence for fluid migration at the seabed (Bayon et al., 2007; 2011; Sultan et al., 2007b; 2010; 2011; Riboulot et al., 2011a); (2) the sedimentation is affected by gravity processes (Sultan et al., 2007a; Garziglia et al., 2010; Ker et al., 2010; Riboulot et al., 2012); and (3) the age and main controlling parameters of regional sedimentation for the late Quaternary are known (Riboulot et al., 2012). The upper-most five depositional sequences of the ENSD were formed during the last ca. 500 kyr BP, in response to glacial/interglacial fluctuations driven by

100-kyr Milankovitch cycles. Fluid seepages are expressed at the seabed by the presence of pockmarks, gas hydrates, mud volcanoes and carbonate constructions (eg. Damuth, 1994; Cohen and McClay, 1996; Hovland et al., 1997; Brooks et al., 2000; Graue, 2000; Deptuck et al., 2003; Sultan et al., 2007; 2010).

This study presents the influence of the overall stratigraphic organization of the ENSD and of a buried landslide on fluid migration and pockmark generation. Based on the combined analysis of industrial 3D seismic data, scattered 2D seismic lines, sedimentological and geotechnical data (Cone Penetration Tests with pore pressure measurements, CPTu) a conceptual model is proposed to present the age of sedimentary units hosting pockmarks, to explain the origin of pockmarks from transient reservoirs at sequence boundaries and to assess the role of a landslide versus gas seeps.

2. Regional setting

2.1 The Niger Delta

The continental margin off the Niger Delta, named ‘Niger Delta’ by oil companies (e.g., Damuth, 1994, Corredor et al., 2005 among others), ‘Niger Delta complex’ (Oomkens, 1974) or ‘Greater Niger Delta area’ (Morley et al., 2011) is undergoing gravity-driven deformation due to the presence of a mobile substratum at the base of the sediment fill (Damuth, 1994; Bilotti and Shaw, 2005; Corredor et al., 2005). This substratum is formed by Early Tertiary overpressured shale deformed since the Oligocene (Wiener et al, 2006).

The continental shelf of the ‘Niger Delta’ is characterized by an extensional zone dominated by large offset listric normal faults (synthetic and antithetic) (Damuth, 1994; Morley and Guerin, 1996). The upper and middle continental slope represent a translational zone (Damuth, 1994) dominated by folding and faulting in response to rapid sedimentation rates and shale remobilization (Doust and Omatsola, 1990; Morley and Guerin, 1996). As the thick stratigraphic column slowly moved downslope (Morley and Guerin, 1996), the lower slope is characterized by a compressional zone (Damuth, 1994) dominated by a series of linear toe-thrusts forming a fold-and-thrust belt. On the Nigerian continental slope, fluid seepage activity is expressed by the presence of pockmarks, gas hydrates, mud volcanoes and carbonate build-ups (Damuth, 1994; Cohen and McClay, 1996; Hovland et al., 1997; Brooks et al., 2000; Graue, 2000; Deptuck et al., 2003; Sultan et al., 2007; 2010; Riboulot et al., 2011a).

2.2 The Eastern Niger Submarine Delta

The study area is on the continental shelf and slope of the ENSD, roughly 65 km offshore, between 150 and 800 m water depth, and it covers 2350 km^2. Three prominent structural folds are formed by shale-cored anticlines expressed by collapse normal faults faintly discernable at the seabed (folds EA, EB, EC, Fig. 1). These shale-cored folds delimit a large corridor where submarine landslides and fluid-migration features are present.

The ENSD consists of a stack of mud-dominated sedimentary sequences separated by marked erosional surfaces on the continental shelf (D10, D20, D30, D40 and D50 from bottom to the top; Fig. 2a). The shelfal unconformities, formed during sea level falls and lowstands, correspond seaward to correlative bounding conformities that have regional extent. The conformities are marked by high amplitude reflectors in seismic data and correspond to thin sedimentary units, deposited during sea level rise periods, relatively coarser-grained than over and underlying sediment (Riboulot et al., 2012).

Pockmarks in the ENSD are related to gas hydrate dissolution/dissociation, dewatering, presence of fault systems, buried mass transport complexes and fluid escape from petroleum reservoirs (eg., Sultan et al., 2010; 2011; Riboulot et al., 2011a). A large number of pockmarks is observed on the bathymetric map above a Mass Transport Complex called NG1 and mapped in Garziglia et al. (2010).

2.3 The NG1 landslide

Previous studies by Garziglia et al. (2010); Ker et al. (2010) and Riboulot et al. (2012) present a large landslide called NG1 buried in the corridor between the three shale-cored folds of the ENSD (Fig. 1). The most proximal deposits of this landslide are at the outer shelf where Riboulot et al. (2012) highlighted the occurrence of shoreface sedimentary prisms deposed during sea level lowstands. NG1 extends down to the mid slope, covering an area of ~ 200 km^2 for an estimated volume of at least ~12 km^3. NG1 affects the whole depositional sequence S2 between the seismic reflectors D10 and D20, the latter being ascribed to a silty/sandy layer deposited during the sea level rise between MIS10.2 and MIS9.3 (Riboulot et al., 2012). The fact that this silty/sandy layer has been disrupted but kept its stratigraphic position suggests that it has undergone little deformation during the emplacement of the NG1 landslide (Ker et al., 2010).

2.4 Seismic signature of gas in marine sediment

The localized accumulation of free gas in marine sediments often yields anomalous seismic signatures, making seismic methods a useful tool for the identification and characterization of the sub-seafloor 'plumbing system' beneath seep sites. Gas may appear as amplitude enhancement or suppression (e.g. Judd and Hovland, 1992; Gay et al., 2007; Netzeband et al., 2010), as well as through the disruption of seismic reflections often referred to as "acoustic turbidity" (e.g. Judd and Hovland, 1992; Schroot and Schüttenhelm, 2003; Mathys et al., 2005; Schroot et al., 2005; Gay et al., 2007; Jones et al., 2010), and/or as "disturbed zones" (Schroot and Schüttenhelm, 2003). Amplitude enhancement of sedimentary or structural features (i.e., "bright spots") may occur when gas preferentially accumulates in highly permeable layers or structural voids such as faults (e.g. Taylor et al., 2000; Tréhu et al., 2004).

The term "gas chimney" is widely used to refer to vertical/sub-vertical regions of suppressed reflectivity (e.g. Gorman et al., 2002; Haacke et al., 2008) or of enhanced reflectivity (e.g. Schroot and Schüttenhelm, 2003; Gay et al., 2007) caused by gas. The presence of gas creates an inflection of seismic reflectors due to a diminution of the acoustic wave velocity. Moreover, the lack of reflection in the chimney may occur due to physical disruption of sedimentary layering by migrating, gas-charged pore fluids (e.g. Davis, 1992; Gorman et al., 2002), or by highly-reflective overlying interfaces that significantly reduce the transmission of energy (e.g. Judd and Hovland, 1992; Garcia-Gil et al., 2002; Sager et al., 2003).

3. Database and Methods

3.1 Geophysical data

The primary source of data is conventional, industrial 3D seismic reflection data provided by TOTAL. These data come from three reprocessed exploration 3D seismic surveys having an inline and crossline spacing of 12.5 m. The dominant frequency of the seismic data is 70 Hz in the upper 100 ms, giving a vertical resolution of ~10.5 m (at a velocity of 1500 ms^{-1}). The bathymetry used to characterize seafloor morphologies is extracted from seafloor-reflector picking within 3D seismic data and has horizontal resolution of 12.5 m (Fig. 1).

Additionally, High Resolution 2D seismic data were acquired during the ERIG3D cruise using the SYSIF, a recently developed deep-towed acquisition system (Marsset et al., 2010; Ker et al., 2010). With acoustic transducers working in the 580-2200 Hz frequency range, and a 15 m long dual channel streamer, the SYSIF provides images of the first 100 ms twtt below seafloor with a resolution of about 0.5 m.

3.2 Seismic attribute analysis

Seismic data were processed on a workstation and the seismic interpretation and attribute analyses were performed with the SISMAGE software developed by TOTAL (Guillon and Keskes, 2004 - Fig. 3 and Appendix A). The 3D seismic data were pre-stack time migrated and short-offset processed. Then, following the identification and initial mapping of key horizons, SISMAGE was used to calculate isopach and attribute maps. Dip and amplitude attributes were extracted along specific horizons. Other maps were obtained by extracting amplitude, coherency and fault attributes from intervals between two horizons. Such an approach requires previous processing of a coherency and fault cube in SISMAGE (Gay et al., 2006b). As summarized by Bull et al. (2009), the analysis of isopach and attribute maps from a geomorphic perspective is key in deciphering the characteristics of depositional units.

3.3 Sediment core data

Calypso piston cores CS18 and CS31 were obtained from the continental slope of the ENSD in 753 and 762 m water depth, respectively (Tab. 1). Sediment core analysis included physical property measurements (gamma density, P-wave velocities, magnetic susceptibility with a Geotek Multi Sensor Core Logger - MSCL), sedimentological description and continuous major element analysis (Ca, Sr, Ti...) with an Avaatech XRF core scanner (Richter et al., 2006). Based on the evaluation of coring parameters during operations using “CINEMA” software (Bourillet et al., 2007), sediment perturbation during coring is considered as negligible. The core data acquired in this study are correlated to seismic reflection profiles and physical and geochemical logs presented in Riboulot et al. (2012).

3.4 In situ geotechnical measurements

In situ geotechnical measurements (Cone Penetration Tests with pore pressure measurements, CPTu) were carried out with the Penfeld penetrometer. This device developed by Ifremer allows to perform piezocone tests as deep as 30 meters below the seafloor (details in Sultan et al., 2010). The Ifremer piezometer (details in Sultan et al., 2011) was also used to measure the *in situ* pore pressure at two different sites during more than one year. Calypso cores, piezocones, and piezometers characteristics are presented in Table 1.

4. Results

4.1 Morphological description of the buried NG1 landslide

The NG1 submarine landslide is located in a corridor delimited to the west and to the east by the shale-cored folds EC and EA respectively, and it is limited by the shale fold EB to the south in about 800 m water depth (Figs. 1, 2 and 3 and Appendix A). The source area of the NG1 landslide is delimited to the north in about 200 m water depth by the shelf edge and growth faults affecting the seabed and described in Damuth (1994) as the extensional zone of the Niger Delta. NG1 is buried under about 120 m of sediment on the upper slope, but the thickness of the overlaying sediments progressively decreases to about 20 m at mid slope on the flank of the shale-cored fold EB. NG1 affects the sedimentary sequence S2 between seismic reflectors D10 (below) and D20 (Fig. 2a). The seismic reflector D10 at the base of NG1 is mostly continuous and concordant with the underlying sedimentary layers (Fig. 2).

The seismic reflector D20 is more discontinuous although always traceable at the top of NG1. In some areas, D20 appears as a sharp, smooth surface, while in other areas it has a rough, hummocky geometry (Figs. 2, 3a and Appendix A1). The discontinuous character of D20 reflector, showing the thin coarser sedimentary unit deposited during a sea level rise period is discontinuous too, demonstrates that the landslide occurred after this highstand period. NG1 body is generally characterized by lower amplitude, more discontinuous and chaotic seismic reflections (Fig. 3b and Appendix A2 and 3). The isopach map of the seismic sequence S2 bounded by reflectors D10 and D20 reveals the complex morphology of NG1 by showing that its thickness varies from about 10 m to 70 m (Fig.3c). By combining analyses of vertical seismic sections, isopach and attribute maps, NG1 can be divided into four major areas from north to south (Fig. 3 and Appendix A):

- Area 1 is the source area at the shelf edge. There the clinoforms of a sedimentary prism show evidence of tilted blocks and loss of sediment (Fig. 2a: close-up view). So a part of the shoreface prism has been reworked after its deposition, but before the deposition of the following shoreface prism entirely preserved under reflector D30.
- Area 2 in the upper slope, close to the shelf edge, is characterized by a substantial overthickening and reworking of sequence S2 (Fig. 3b and c and Appendix A2 and A3).
- Area 3 shows sharp lateral variations (from west to east) in thickness and seismic facies allowing to distinguish a western, a central and an eastern unit (Figs. 2b, 3 and 4a).
- Area 4 represents the distal part of NG1 on the flank of the shale-cored fold EB. There the sequence S2 is also substantially overthickened.

Seismic analysis suggests that the degree of sediment deformation in Area 4 is comparable to that of Area 2 and of the western and eastern units of Area 3. Area 3 constitutes the main part of the landslide deposit on the upper continental slope. Its *central unit* has a homogeneous seismic facies with evident layering and without faults (Figs. 2b, 3a and Appendix A3). The seismic facies is coherent/consistent (Fig. 3b). The two lateral units, the *western unit* and the *eastern unit*, display two convex-downslope lobe like geometries (Figs. 2b and 3). Based on the analysis of isopach, coherency and fault attribute maps, it is in these lobes that the most severe deformation occurred. A far lower degree of deformation can be inferred from the homogeneous, layered seismic facies characterizing the central unit of Area 3. Moreover, the seismic reflectors at the top (D20) and base (D10) of NG1 are of higher amplitude in the central unit than in the two bounding lateral units. It is also noteworthy that the central unit is comparable in thickness to undisturbed sediment out of the landslide (Figs. 2b, 3c and Appendix A1).

4.2 Silty/sandy layers below and above NG1

The 2D HR seismic profiles show several reflectors characterized by high amplitude corresponding to correlative conformities of sequence boundaries identified on the shelf (Fig. 5a and Appendix B). Reflectors D10, D30 and D40 are relatively continuous with local interruptions due to fluid chimneys, while D20 is a discontinuous reflector at the top of NG1 landslide deposit (Fig. 5a and Appendix B). The D10 seismic signature is similar to signatures of enhanced reflections caused by lateral and vertical fluid migration described in the literature (e.g., Sun et al., 2012 and references therein).

In situ piezocone data show that the high amplitude reflectors D10 and D20 correspond to silty/sandy layers because they are characterized by high tip resistance, high friction and low pore pressure (see CPT09S07 and CPT09S08 data in Fig. 5). The reflector D40 is not detected by in situ piezocone data.

Calypso core CS18 intersects the regional reflector D40 and shows that its high amplitude can be correlated to a silty/sandy layer at 7 mbsf. The gamma density of this silty/sandy layer measured in the core is 1.650 g.cm^{-3}. Figure 5a shows that core CS18 reaches NG1 deposits below reflector D20 marking its top at 17 mbsf. In agreement with piezocone results, core analysis reveals that D20 reflector corresponds to a silty/sandy layer (Fig. 5a).

The calypso core CS31 (10.56 m long) was collected outside NG1 (Fig. 5 and Appendix B). By contrast to the observations made on core CS18, the presence of a silty/sandy layer at 10 mbsf in core CS31 cannot be correlated to the seismic reflector D40, which intersects the core at about 8 mbsf. The gamma density of the silty/sandy layer measured in the core has relatively low values (1.500 g.cm^{-3}; Fig. 6b), probably due to its thinning on the eastern flank of fold EB: this same interpretation could account for the lack of expression of D40 in piezocone CPT09S08 close to core CS31.

4.3 Pockmarks

Pockmarks occur in an area of 175 km^2 between folds EA and EC in water depth of 500 to 700 m. Some 376 pockmarks reach the seafloor, while 155 pockmarks are buried. They are all regular circular features with diameter of several tens of meters (Figs. 4b, 4c and 6). They vary in diameter from several meters to a maximum of 200 m, while the depth of the depression at the seafloor may reach 25 m. The pockmark density in the study area is approximately 2.15/km^2, higher than the concentration described by Pilcher and Argent, (2007) on the west African continental margin, but lower than densities described in other areas (e.g., Fader, 1991; Foland et al., 1999; Hovland and Judd, 1988).

In the study area, we distinguish three groups of pockmarks based on their distribution and origin: 1) random pockmarks (RP) deeply rooted in the sedimentary column; 2) random pockmarks rooted in the conformity surface D40; and 3) non-random pockmarks (NRP) in connection with the NG1 landslide (Fig. 6d).

4.3.1 Deeply rooted random pockmarks

We identified as random pockmarks 114 out of the 531 pockmarks present in the study area (21% of the total number of pockmarks). Random pockmarks are regular cone-shaped pockmarks with a diameter ranging from 10 to 200 m. Some of them occur at the seafloor while other are buried (Fig. 4c). Most of these pockmarks occur in the southern portion of Area 3 and they are restricted to areas affected in depth by small shale folds (Fig. 6c). They seem rooted on these small folds. Some chimneys associated to the random pockmarks cross the NG1 landslide, others terminate in the sedimentary layers underlying NG1 (Fig. 6c). The vertical chimney of this group of pockmarks can be up to 200 m high. Chimneys are characterized by a downward deflection or an interruption of seismic reflectors.

4.3.2 Random pockmarks linked to the D40 reflector

We count 263 pockmarks out of the 531 in the study area (49% of the total number of pockmarks of the study area) that affect only the youngest sequence S5 with chimneys rooted in the D40 reflector. These pockmarks are similar in morphology to all the others, but have smaller sizes; their diameters range from 10 to 100 m with a depth less than 10 m (Figs. 4 and 6). Vertical chimneys of this group of pockmarks cross-cut the whole sedimentary sequence S5 so they are about 50 m high. Chimneys are characterized by downward deflections and low amplitudes of seismic reflectors. The 2D HR seismic dataset provides better images of pockmark chimneys that are undoubtedly rooted in the D40 reflector (Fig. 7 and Appendix B).

4.3.3 Non-random pockmarks linked to NG1

A series of NW-SE alignments of pockmarks matches with the perimeter and the internal structure of NG1 landslide (Fig. 4c). These pockmarks are rooted in the discontinuities present within the NG1 landslide, at the limits between the western, central and eastern NG1 internal units and may either reach the seafloor or end in the D40 reflector (Fig. 6). Non-random pockmarks linked to NG1 are sub-circular seafloor depressions corresponding in depth to seismic reflector packages with a local downward deflection. Their crater has a diameter of 10 to 140 m with a depth of about ten meters.

In total we note 154 pockmarks, 29% of the total number of pockmarks of the study area, whose chimney begins in discontinuities within NG1 landslide at the contact between the three internal units (Western, Central, and Eastern). Of these 154 pockmarks, 85 are rooted at the transition between NG1 and the surrounding sediments, that is along NG1 perimeter, while 69 originate in correspondence with the limits of the internal units (Fig. 4c). In addition, of these 154 pockmarks, 87 end up on the surface D40 and 67 at the seabed.

Chimneys of this group of pockmarks are characterized by a downward deflection or an interruption of seismic reflectors associated to an alternation of low and high amplitude anomalies in the center of the chimneys (Fig. 6). Figure 7 shows more precisely the rooting of the chimney in NG1 landslide. The chimney of the non-random pockmark appears transparent with an interruption of seismic reflectors between D20 and D40. At D40, the pockmarks observed in this seismic section are completely infilled. The chimney of the last sequence rooted in the upstream flank of the D40 pockmark is characterized by an inflection of the seismic reflectors. The observations about the repartition of pockmarks in the sedimentary column are summarized in Figure 6d.

4.4 Piezometer data description and interpretation

Long-term piezometers deployed at PZS13 and PZS14 sites (Figs. 1, 5 and Appendix B) aimed to detect any potential fluid activities in the most frontal part of NG1, where deformation processes are active today (Garziglia et al., 2010). PZS13 and PZS14 data are presented in Figure 8 and show relatively limited pore pressure fluctuations during the almost 1-year long monitoring period. However, data from Figure 8 confirm the presence of free gas at the top of NG1. In fact, piezometer data show that at given locations pore pressure perturbations occur in 12-hours cycles and 15-days cycles. The pore pressure fluctuates with semi-diurnal tides and with the spring/neap tides. It is important to mention that the tidal cycles effect on differential pore pressure sensors is an indication of the increase of the compressibility of the pore fluid and, therefore, demonstrates the presence of free gas in the pore fluid. Figure 8 shows that free gas is present at levels P3, P4 and P5 for PZS 13 and levels P2, P3, P4 and P5 for PZS14.

For PZS13, pore pressure fluctuations generated by the 15-days tidal cycle recorded by P3, P4 and P5 show that the highest amount of free gas occurs at P3 (Fig. 8a) which fits with the D40 reflector (see Fig; 5 and Appendix B).

Data recorded by PZS14 (Fig. 8b) show the 15-days tidal cycle recorded by P2 to P4. Here, the highest amount of free gas occurs at P4 and P5, which are located around D10 and D20 reflectors. Moreover, pore pressure increases during almost two months at P2 level (between the 27th of May and the 29th of July 2008 – Fig. 8b). The fluid accumulation is followed by long-term, smooth pore-pressure dissipation (between the 29th of July and the 1st of October 2008). The P1 sensor of PZS14 has recorded during almost the same period (14th of June to

1st of October 2008) a small depression (pressure lower than hydrostatic) which may indicate gas bubbles rising up and generating a decrease of the hydrostatic pressure due to the low gas density.

5. Discussion

5.1 The role of silty/sandy layers in muddy successions

A thin permeable silty/sandy layer between two layers that have very low permeability could act as a reservoir of fluid or preferential fluid conduit as it was suggested in the eastern flank of the shale-cored anticlines EB (Sultan et al., 2011). There are two possible transient storage zones of gas in the study area based on seismic data, sediment cores and in situ piezocone and piezometer measurements: (1) the first reservoir is located under the NG1 landslide and corresponds to the silty/sandy sedimentary unit marked by reflector D10 (Figs. 5a and 6); (2) the second reservoir is formed by the coarse grain-size sedimentary layer marked by seismic reflector D40 on seismic data but the very high resolution of the seismic line presented in figure 7 show this layer is above the reflector D40. This upper reservoir is marked in 3D seismic data by a very high amplitude reflector (Figs. 2, 4 and 6), in core and CPTu data by a silty/sandy layer and in piezometer data by the presence of free gas. This layer was deposited during the sea level rise that followed the MIS 6 glacial interval (Riboulot et al., 2012).

5.2 The interplay of NG1 landslide and fluids within sediment

Data presented in this study complete the interpretations of Garziglia et al., 2010 and Ker et al., 2010 and suggest a possible link between fluid dynamics and NG1 landslide. Some lines of evidence in support of this link are listed below:

- Pockmarks are localized in the most deformed area of NG1 and at the discontinuities between the NG1 internal units (Fig. 4c). Indeed, the Area 3 of NG1 in the upper continental slope is composed of three units. The central unit is much less affected by deformation than the two peripheral units: it is layered and underwent a translational motion to the south without changing its original structure. The internal discontinuities between the three parts are the preferential pathways for fluid migration.

- NG1 landslide overlays a silty/sandy permeable layer (seismic reflector D10) with evidence (piezometer and seismic data interpretation) of fluid circulations and free gas occurrences (Figs. 5, 6, 8 and Appendix B). This basal layer, covered by impermeable shale layer, can play the role of gas storage area.
- Sediment failure of NG1 landslide occurs during sea level fall where free and dissolved gas may generate important excess pore pressure due to gas exsolution and expansion, with a mechanism that could be similar to that proposed for Ana Slide in the Balearic Islands (Lafuerza et al. 2012).

Fluids use preferential migration pathways such as discontinuities created by a landslide to migrate to the surface as outlined by the geographical distribution of the pockmarks rooted in the NG1 landslide (Fig. 4C) and the rooting of many chimneys in NG1 landslide (Fig. 7). This is consistent with models for pockmark conduits as pipe-like zones of enhanced fracturing (Cartwright et al., 2007; Moss and Cartwright, 2010; Løseth et al., 2011), where certain hydrodynamic conditions dynamically re-open pathways from the available fracture network permitting a renewed phase of focused fluid expulsion and pressure bleed-off (Moss et al., 2012). Submarine landslide deposits can influence fluid circulation within the sediments in various ways: they can release their intrinsic fluids, play the role of impermeable caprock of fluid reservoir (Plaza-Faverola et al., 2010; Dugan, 2012), play the role of gas storage zone (Sun et al., 2012), or create preferential pathways for focused fluid flow (Bayon et al., 2009). Landslide deposits may have low porosity in comparison to the encasing hemipelagic sediments, and may thus result in enhanced consolidation related to shear deformation (Dugan, 2012). Our observations and interpretations show that NG1 landslide deposit has both played the role of impermeable caprock and created discontinuities in sedimentary layers acting as preferential migration pathway for gas to migrate to the surface: this fact depends on the intrinsic small-scale variability and complexity of landslide deposits. It can be noted that vertical chimneys, rooted in NG1 and ending in D40 (Fig. 7), can form a high-permeable vertical zone, analogous to what is called a “seal bypass system” (Cartwright et al., 2007), where fluids and gas can be transported faster than would otherwise be allowed by the normal permeability in the pore network of the sediments. High fluid overpressure opening a hydro fracture through low permeable sediments is a common first phase of all these bypass structures (Arntsen et al., 2007; Cartwright et al., 2007; Løseth et al., 2009; Rodrigues et al., 2009).

5.3 The role of sea level fluctuations

Many studies suggest that landslides occurred during periods of rapid sea-level rise (e.g. Maslin et al., 2004; Quidelleur et al., 2008; Georgiopoulou et al., 2010; McGuire, 2010; Smith et al., 2011). Maslin et al. (2004) maintained that, based on landslide volume, 70% of continental slope failures during the last 45,000 years occurred in periods of rapid sea-level rise. Certainly, the time distribution of submarine landslides is uneven, more frequent during or shortly after the last glacial/deglaciation period and probably dominated by glacial cycles and related phenomena (Lee, 2009). Landslides triggered during sea level fall period include among others Ana Slide (Berndt et al., 2012; Lafuerza et al., 2012) and the present study. The spatial match between the NG1 landslide and fluid flow indicators strongly suggests that fluid migration has played a role in the destabilization of slope sediments in the ENSD, and reminds of previously suggested relationships between repeated destabilization and fluid flow in the Eivissa Channel (Berndt et al., 2012; and references therein). This relationship was proposed also for the Storegga Slide off mid-Norway, where the most deeply incised slope failures occur precisely above a leaking gas reservoir (Bünz et al., 2005). A plausible mechanism at the origin of the NG1 event could be the presence of free and dissolved gas in the basal silty/sandy layers marked by D10 reflector. The decrease of hydrostatic pressure generated by sea level fall could have induced an important increase in pore pressure and therefore an important decrease of the effective stress. The shear strength of sands is directly linked to the effective stress (no cohesion), and an important decrease of the effective stress can cause sediment to slide even with an extremely reduced initial slope. Indeed, pore pressure accumulation may cause liquefaction of sand.

The main cause of overpressure generation on passive margins is disequilibrium compaction due to rapid and high sedimentation (eg. Flemings et al., 2008; Talukder, 2012). In most cases, the generated overpressure is not sufficient to induce hydrofracturing in the overburden to initiate focused fluid flow. This requires external factors, and tectonic stress appears to be the most efficient trigger mechanism for seeps (Talukder, 2012). The overpressure could be due to sea level fall (Lafuerza et al., 2009). Recent studies suggest the possible impact of sea level changes to explain the origins of pockmarks (Lafuerza et al., 2009; Hammer et al., 2010; Andresen et al., 2011; Plaza-Faverola et al., 2011). Sea-level fall appears to be the most efficient trigger mechanism for pockmark formation as it was suggested in the Lower Congo Basin (Andresen et al., 2011) and in the Nyegga region, offshore Norway (Plaza-Faverola et al., 2011) where pockmark activity appear to coincide with sea-level fall periods. Indeed, relative sea-level changes modify hydrostatic pressure: when the sea level falls, gas volume in fluid reservoir increases, and the formation of gas bubbles may induce pockmark formation (Lafuerza et al., 2009).

Riboulot et al., (2011b) show that late Quaternary sea-level changes with 100-ky cyclicity are one of the main driving factors in pockmark formation in the Gulf of Lions and possibly elsewhere. This control of 100-ky cyclicity in pockmarks development is deduced from the observation that pockmarks affect well-identified and discrete stratigraphic units and function episodically during the final phase of lowstand periods and the onset of sea level rise (Riboulot et al., 2011b). Also in the ENSD most of the observed pockmarks are present within stratigraphic units bounded by surfaces that correspond to times of sea-level changes (and in particular of sea level fall; Figs. 6a and 7). The drop in sea level of about 100 m during the Marine Isotope Stage 6 could be the cause of overpressure in gas storage zones underlying the NG1 landslide, which creates a fracture in the overlying sedimentary layers or reactivate pre-existing discontinuities like those creating by the NG1 gravity sliding. Pockmark formation may occur in the catastrophic way initially proposed by Hovland (1987). The same process during the Marine Isotope Stage 2 could originate pockmarks observed at the seabed and rooted either in D40 or in D10 surfaces.

5.4 Model of pockmark formation linked to a landslide

For the formation of pockmarks above the NG1 landslide, we propose a scenario consisting of five phases taking into account temporary gas storage, preferred pathways of gas migration, the role of sediment deformation and failure, and the influence of relative sea-level changes.

Phase 1 (Fig. 9a) - The origin of pockmark formation is linked to the presence of faults crossing gas-bearing sedimentary units, similarly to what has been proposed elsewhere by several independent studies (e.g., Papatheodorou et al. 1993; Boe et al. 1998; Soter, 1999; Pilcher and Silver, 2007; Forwick et al., 2009). This process can cause the formation of two types of pockmarks: the fault-strike pockmarks and the fault hanging-wall pockmarks (Pilcher and Silver, 2007).

Phase 2 (Fig. 9b) - A condensed layer is formed during sea level rise on top of lowstand shoreface prisms and coeval distal marine deposits. After burial, the condensed layer with grain size coarser than encasing sediment becomes a potential fluid reservoir. This is the case, for example of the condensed unit marked in seismic data by the reflector D10.

Phase 3 (Fig. 9c) - During the following sea level fall, the decrease of the hydrostatic pressure in the transient fluid reservoir above D10 induce an important increase of the pore pressure and therefore an important decrease of the effective stress. This layer becomes a weak layer; a part of the continental slope is destabilized reaching the outer shelf. The NG1 landslide has a complex internal organization with distinct less permeable units (due to partial reworking of sediments during sliding) and discontinuities between the units that constitute preferential paths for fluid escape.

Phase 4 (Fig. 9d) - After two 100 kyr climatic cycles, the landslide is buried and the underlying sedimentary layer has charged again in gas. During the lowstand MIS 6.2, many pockmarks are formed through the discontinuities created by the NG1 landslide. The presence of a landslide deposit with less permeable layers and internal discontinuities may influence both gas pressure increase, and gas release through preferential paths. The presence of a landslide becomes the controlling factor of the non random organization of pockmarks.

Phase 5 (Fig. 9e) - During the lowstand MIS2.2, the mechanism of pockmark formation linked to NG1 is the same as in Phase 4. In addition, the migration of gas through the NG1 discontinuities feeds a second transient fluid reservoir. The layer above D40 acts as a source area for random pockmark formation affecting the uppermost sequence S5. Two generations of pockmarks (linked to NG1 landslide and to the layer above D40) show a marked stratigraphic segregation.

6. Conclusions

While pockmarks have been recognized in many zones of the African coast, we extend the known range of formation processes of these features in three ways: 1) we show the relevance of the knowledge of the stratigraphic context (stratigraphic units and their age) where pockmarks are present to understand their timing and mode of functioning; 2) we link the spatial distribution and origin of pockmarks to well identified buried features: the presence of a landslide represents the main controlling factor of non random spatial organization of pockmarks in the study area; and 3) we propose that sea level changes are the main controlling factor for the timing of pockmarks formation. The timing of pockmark formation is in part exclusively controlled by 100-ky cyclicity, in part dependent (for deeply rooted pockmarks) on the presence of deep structures.

Pockmarks observed in the Eastern Niger Submarine Delta (ENSD) include pockmarks rooted in a large buried submarine landslide and pockmarks linked to coarser grain size sedimentary layers formed during phases of sea-level rise. The pockmarks above the buried NG1 landslide are similar in morphological terms, but can be broadly distinguished in three well identified groups: 1) deeply-rooted random pockmarks whose chimneys end under NG1 landslide or at the seafloor; 2) non-random pockmarks linked to the NG1 landslide (reaching the seafloor and/or ending within D40); and 3) random pockmarks rooted in D40 reflector marking the presence of a coarser sedimentary layer.

The integrated study of pockmarks provides the first detailed evidence of the implication of a landslide into the development of a pockmark field. The spatial distribution of pockmarks can be controlled by a buried landslide deposit in a comparable way of pockmark alignments depending on underlying channels. The processes of pockmark formation imply the concomitant action of several factors: (1) a gas source, (2) preferential gas migration pathways, (3) gas accumulation zones and (4) global sea-level change.

Our results provide useful information about the role of sea level changes and indirectly climate change on gas seeps: gas release intensification during sea level lowstand can have relevant implication on global warming after ice ages.

Acknowledgements

This work has been developed and funded by Ifremer and Total, through the ERIG3D project. The support by officers and crew during the ERIG3D cruise on board R/V “Pourquoi Pas ?” (2008) is greatly appreciated, as is the dedication of the Genavir and Ifremer technical staff during the cruise. The identification of the nature of the pockmarks and the mapping of the NG1 landslide would have been impossible without the use of reprocessed exploration 3D seismic kindly provided by TOTAL and TOTAL Nigeria Subsidiary. We also thank Bruno Marsset (Ifremer) and Eric Cauquil (Total) for reviewing the manuscript and providing insightful comments. We thank sincerely the reviewers J. Cartwright and C. Berndt, and the editor P. Shearer for their stimulating comments and suggestions.

References

Abrams, M.A., 1992. Geophysical and geochemical evidence for subsurface hydrocarbon leakage in the Bering Sea, Alaska. Mar. Pet. Geol. Bull. 9, 208-221.

Andresen, K.J., et al. 2008. Morphology and distribution of Oligocene and Miocene pockmarks in the Danish North Sea -implications for bottom current activity and fluid migration. Basin Res. 20, 445-466.

Andresen, K.J., Huuse, M., 2011. ‘Bulls-eye’ pockmarks and polygonal faulting in the Lower Congo Basin: Relative timing and implications for fluid expulsion during shallow burial. Mar. Geol. 279, 111-127.

Arntsen, B., et al. 2007. Seismic modelling of gas chimneys. Geophysics 72, 251-259.

Bayon, G., et al. 2011. Evidence for intense REE scavenging at cold seeps from the Niger Delta margin. Earth Planet. Sci. Lett. 312, 443-452, doi:10.1016/j.epsl.2011.10.008.

Bayon, G., et al. 2009. Multidisciplinary investigation of fluid seepage on an unstable margin: the case of the Central Nile deep sea fan. Mar. Geol. 261, 92-104.

Bayon, G., et al. 2007. Sr/Ca and Mg/Ca ratios in Niger Delta sediments: Implications for authigenic carbonate genesis in cold seep environments. Mar. Geol. 241, 93-109.

Berndt, C., et al. 2012. Repeated slope failure linked to fluid migration: The Ana submarine landslide complex, Eivissa Channel, Western Mediterranean Sea. Earth Planet. Sci. Lett. 319-320, 65-74, doi:10.1016/j.epsl.2011.11.045.

Bilotti, F.D., Shaw, J.H., 2005. Deepwater Niger Delta fold and thrust belt modelled as a critical-taper wedge: the influence of elevated of elevated basal fluid pressure on structural styles. AAPG Bull. 89, 1475-1491.

Boe R, et al. 1998. Elongate depressions on the southern slope of the Norwegian Trench (Skagerrak): morphology and evolution. Mar. Geol. 146, 191-203.

Bourillet, J.F., et al. 2007. Behaviour of a piston corer from accelerometers and new insights on quality of the recovery. Proceedings of the 6th International Offshore Site Investigation and Geotechnics Conference: Confronting New Challenges and Sharing Knowledge, 11-13 September 2007, London, UK, 57-62.

Brooks, J.M., et al. 2000. The nature of gas hydrates on the Nigerian continental slope. Gas hydrates:Challenges for the future. Ann. N.Y. Acad. Sci. 912, 76-93.

Brown, A., 2000. Evaluation of possible gas microseepage mechanisms. AAPG Bull. 84 (11), 1775-1789.

Bull, S., et al. 2009. A review of kinematic indicators from mass-transport complexes using 3D seismic data. Mar. Pet. Geol. 26, 1132-1151.

Bünz, S., et al. 2005. Fluid flow impact on slope failure from 3D seismic data: a case study in the Storegga Slide. Basin Res. 17, 109-122.

Cartwright, J., et al. 2007. Seal bypass systems. AAPG Bull. 91, 1141-1166.

Cathles, L.M., et al. 2010. The physics of gas chimney and pockmark formation, with implications for assessment of seafloor hazards and gas sequestration. Mar. Pet. Geol. 27, 82-91.

Cohen, H.A., McClay, K., 1996. Sedimentation and shale tectonics of the northwestern Niger Delta front. Mar. Pet. Geol. 13, 313-328.

Corredor, F., et al. 2005. Structural styles in the deep-water fold and thrust belts of the Niger Delta. AAPG Bull. 89, 753-780.

Damuth, J.E., 1994. Neogene gravity tectonics and depositional processes on the deep Niger Delta continental margins. Mar. Pet. Geol. 11, 321-346.

Davis, A.M., 1992. Shallow gas: an overview. Cont. Shelf Res. 12 (10), 1077-1079.

Deptuck, M.E., et al. 2003. Architecture and evolution of upper fan channel belts on the Niger Delta slope and in the Arabian Sea. Mar. Pet. Geol. 20, 649-676.

Dimitrov, L., Woodside, J., 2003. Deep sea pockmark environments in the eastern Mediterranean. Mar. Geol. 195, 263-276.

Doust, H., Omatsola E., 1990. Niger Delta. In: Edwards, J.D., Santogrossi, P.A. (Eds.), Divergent/passive margin basins. AAPG Mem. 48, 201-238.

Dugan, B., 2012. Petrophysical and consolidation behavior of mass transport deposits from the northern Gulf of Mexico, IODP Expedition 308, Mar. Geol. doi:10.1016/j.margeo.2012.05.001.

Eichhubl, P., et al. 2000. Structural control of fluid flow: offshore fluid seepage in the Santa Barbara Basin, California. J. Geochem. Explor. 69-70, 545-549.

Fader, G.B.J., 1991. Gas-related sedimentary features from the eastern Canadian continental shelf Cont. Shelf Res. 11, 1123-1153

Flemings, P.B., et al. 2008. Pore pressure penetrometers document high overpressure near the seafloor where multiple submarine landslides have occurred on the continental slope, offshore Louisiana, Gulf of Mexico. Earth Planet. Sci. Lett. 274(1-2), 269-283.

Foland, S.S., et al. 1999. Pockmarks along the Californian Continental Margin: implications for fluid flow. Abstract. AAPG Bull. 83, 681-706.

Forwick, M., et al. 2009. Pockmarks in Spitsbergen fjords. Nor. J. Geol. 89, 65-77, ISSN 029-196X.

Garcia-Gil, S., et al. 2002. Shallow gas features in incised-valley fills (Ria de Vigo, NW Spain): a case study. Cont. Shelf Res. 22, 2303-2315.

Garziglia, S., et al. 2010. Identification of shear zones and their causal mechanisms using a combination of cone penetration tests and seismic data in the Eastern Niger Delta. In: Mosher, D., et al. (Eds.), Submarine Mass Movements and Their Consequences - Advances in Natural and Technological Hazards Research. Springer 28, 55-65.

Gay, A., 2002. Les marqueurs géologiques de la migration et de l'expulsion des fluides sédimentaires sur le plancher des marges passives matures. Exemples dans le Bassin du Congo. Thèse de doctorat, Université de Lille 1, 426 pp.

Gay, A., et al. 2007. Geological controls on focused fluid flow associated with seafloor seeps in the Lower Congo Basin. Mar. Geol. 244 (1-4), 68-92.

Gay, A., et al. 2006a. Evidences of early to late fluid migration from an upper Miocene turbiditic channel revealed by 3D seismic coupled to geochemical sampling within seafloor pockmarks, Lower Congo Basin. Mar. Pet. Geol. 23, 387-399.

Gay, A., et al. 2006b. Isolated seafloor pockmarks linked to BSRs, fluid chimneys, polygonal faults and stacked Oligocene-Miocene turbiditic palaeochannels in the Lower Congo Basin. Mar. Geol. 226, 25-40.

Georgiopoulou, A.D.G., et al. 2010. Sahara Slide: Age, initiation, and processes of a giant submarine slide. Geochem. Geophys. Geosyst., 11, Q07014, doi:10.1029/2010GC003066.

Gorman, A.R., et al., 2002. Migration of methane gas through the hydrate stability zone in a low-flux hydrate province. Geology 30 (4), 327-330.

Graue, K., 2000. Mud volcanoes in deepwater Nigeria. Mar. Pet. Geol. 17, 959-974.

Guillon, S., Keskes, N., 2004. Sismage and the 3D Visualization at TOTAL. AAPG Int. Conf.: October 24-27, 2004; Cancun, Mexico. 3 pp.

Haacke, R.R., et al. 2008. High-flux gas venting in the East Sea, Korea, from analysis of 2D seismic reflection data, 6th International Conference on Gas Hydrates (ICGH 2008), Vancouver. British Columbia, Canada.

Hammer, O., Webb, K.E., 2010. Piston coring of Inner Oslofjord Pockmarks, Norway: constraints on age and mechanism. Nor. J. Geol. 90, 79-91.

Harrington, P.K., 1985. Formation of pockmarks by porewater escape, Geo-Mar. Lett. 5 (3), 193-197.

Hovland, M., 1983. Elongated depressions associated with pockmarks in the western slope of the Norwegian trench. Mar. Geol. 51, 35-46.

Hovland, M., 1987. The formation of pockmarks and their potentiel influence on offshore construction. Proc. of JSCE, 388/III-8 (Geotechnical eng.), 13-22.

Hovland, M., 1991. Large pockmarks, gas-charged sediments and possible clay diapirs in the Skagerrak. Mar. Pet. Geol. 8, 311-316.

Hovland, M., Gallagher, J.W., 1997. Gas hydrate and free gas volumes in marine sediments: Example from the Niger Delta front. Mar. Pet. Geol. 14, 313-328.

Hovland, M., et al. 2002. The significance of pockmarks to understanding fluid flow processes and geohazards. Geofluids 2, 127-136.

Hovland, M., Judd, A. G. 1988. Seabed pockmarks and seepages: Impact on geology, biology and the marine environment. London: Graham and Trotman 293 pp.

Hovland, M., et al. 1984. Characteristic features of pockmarks on the north sea floor and scotian shelf. Sedimentology 31, 471-480.

Hovland, M., et al. 2005. Complex pockmarks with carbonate-ridges off mid-Norway: Products of sediment degassing. Mar. Geol. 218, 191-206.

Hustoft, S., et al. 2007. High-resolution 3D-seismic data indicate focussed fluid migration pathways above polygonal fault systems of the mid-Norwegian margin. Mar. Geol. 245 (1-4), 89-106.

Jones, A.T., et al. 2010. Acoustic and visual characterization of methane-rich seabed seeps at Omakere Ridge on the Hikurangi Margin, New Zealand. Mar. Geol. 272,154-169.

Josenhans, H.W., et al. 1978. A side-scan sonar mosaic of pockmarks on the Scotian shelf. Can. J. Earth Sci. 15, 831-840.

Judd, A.G., Hovland, M., 1992. The evidence of shallow gas in marine sediments. Cont. Shelf Res. 12, 1081-1095.

Ker, S., et al. 2010. High-resolution seismic imaging in deep sea from a joint deep-towed/OBH reflection experiment: application to a Mass Transport Complex offshore Nigeria. Geophys. J. Int. 182, 1524-1542, doi:10.1111/j.1365-246X.2010.04700.x

King, L.H., MacLean, B., 1970. Pockmarks on the Scotian shelf. Geol Soc. Am. Bull. 81, 3141-3148.

Lafuerza, S., et al. 2009. Overpressure within upper continental slope sediments from CPTU data, Gulf of Lion, NW Mediterranean Sea. Int. J. Earth Sci. (Geol Rundsch), doi:10.1007/s00531-008-0376-2.

Lafuerza, S., et al. 2012. Failure mechanisms of Ana Slide from geotechnical evidence, Eivissa Channel, Western Mediterranean Sea. Mar. Geol. 307-310, 1-21, doi:10.1016/j.margeo.2012.02.010.

Lee, H.J., 2009. Timing of occurrence of large submarine landslides on the Atlantic Ocean margin. Mar. Geol. 264, 53-64.

Løseth, H., et al. 2009. Hydrocarbon leakage interpreted on seismic data. Mar. Pet. Geol. 26, 1304-1319.

Løseth, H., et al. 2011. 1000 m long gas blow-out pipes. Mar. Pet. Geol. 28, 1040-1060.

Marsset, T., et al. 2010. High and very high resolution deep-towed seismic system: Performance and examples from deep water Geohazard studies. Deep-Sea Res. Part I, 57(4), 628-637, doi:10.1016/j.dsr.2010.01.001.

Maslin, M.A., et al. 2004. Linking continental slope failure to climate change: testing the clathrate gun hypothesis. Geology 32, 53-56.

Mathys, M., et al. 2005. Seismic characterisation of gas rich near surface sediments in the Arkona Basin, Baltic Sea. Mar. Geophys. Res. 26, 207-224.

McGuire, B., 2010. Potential for a hazardous geospheric response to projected future climate changes. Phil. Trans. R. Soc. A. 368, 2317-2345, doi:10.1098/rsta.2010.0080.

Morley, C.K., Guerin G., 1996. Comparison of gravity-driven deformation styles and behavior associated with mobile shales and salt. Tectonics 15, 6, 1154-1170.

Morley, C.K., et al. 2011. Deepwater fold and thrust belt classification, tectonics, structure and hydrocarbon prospectivity: a review. Earth-Sci. Rev. 104, 41-91.

Moss, J.L., Cartwright, J., 2010. 3D seismic expression of km-scale fluid escape pipes from offshore Namibia. Basin Res. 22, 481-501.

Moss, J.L., et al. 2012. The spatial pattern and drainage cell characteristics of a pockmark field, Nile Deep Sea Fan. Mar. Pet. Geol. 35, 321-336.

Netzeband, G.L., et al. 2010. The structures beneath submarine methane seeps: Seismic evidence from Opouawe Bank, Hikurangi Margin, New Zealand. Mar. Geol. 272, 57-70

Oomkens,E., 1974. Lithofacies relations in the Late Quaternary Niger Delta complex. Sedimentology 21, 195-222.

Papatheodorou, G., et al. 1993. Gas-charged sediments in the Aegean and Ionian Seas, Greece. Mar. Geol. 112, 171-184.

Paull, C., et al. 2002. Pockmarks off Big Sur, California. Mar. Geol. 181, 323-335.

Pilcher, R., Argent, J., 2007. Mega-pockmarks and linear pockmark trains on the West African continental margin. Mar. Geol. 244, 1-4, 15-32.

Plaza-Faverola, A., et al. 2010. Fluid distributions inferred from P-wave velocity and reflection seismic amplitude anomalies beneath the Nyegga pockmark field of the mid-Norwegian margin. Mar. Pet. Geol. 27, 46-60.

Plaza-Faverola, A., et al. 2011. Repeated fluid expulsion through sub-seabed chimneys offshore Norway in response to glacial cycles. Earth Planet. Sci. Lett. 305, 297-308, doi:10.1016/j.epsl.2011.03.001.

Quidelleur, X., et al. 2008. Causal link between Quaternary palaeoclimatic changes and volcanic islands evolution. J. Geophys. Res. 35, L02303, doi:10.1029/2007GL031849.

Rao, Y., et al. 2001. Anomalous seismic reflections related to gas/gas hydrate occurences along the western continental margin of India. Geo-Mar. Lett. 21, 1-8.

Riboulot V., et al. 2012. Geometry and chronology of late Quaternary depositional sequences in the Eastern Niger Submarine Delta. Mar. Geol. 319-322, 1-20, doi:10.1016/j.margeo.2012.03.002.

Riboulot, V., et al. 2011a. Morphological signature of fluid flow seepage in the Eastern Niger Submarine Delta (ENSD). Houston, TX, USA. OTC 21744.

Riboulot, V., et al. 2011b. Obliquely migrating pockmarks formed in response to 100 kyr and millennial-scale sea-level changes in the Gulf of Lions (Western Mediterranean), European Geosciences Union, 03-08 April 2011, Vienna, Austria, Abstract, 10295.

Richter, T.O., et al. 2006. The Avaatech XRF Core Scanner: technical description and applications to NE Atlantic sediments. In: Rothwell, R.G. (Ed.), New Techniques in Sediment Core Analysis. Geol. Soc. Spec. Publ. 267, 39-50.

Rodrigues, N., et al., 2009. Physical modelling of sand injectites. Tectonophysics 474, 610-632.

Sager, W.W., et al. 2003. Geophysical signatures of mud mounds at hydrocarbon seeps on the Louisiana continental slope, northern Gulf of Mexico. Mar. Geol. 198, 97-132.

Schroot, B.M., et al. 2005. Surface and subsurface expressions of gas seepage to the seabed-examples from the Southern North Sea. Mar. Pet. Geol. 22 (4), 499-515.

Schroot, B.M., Schüttenhelm, R.T.E., 2003. Expressions of shallow gas in the Netherlands North Sea. Neth. J. Geosci. 82 (1), 91-105.

Smith, D.E., et al. 2011. The early Holocene sea level rise. Quaternary Sci. Rev. 30, 15-16, 1846-1860.

Soter, S., 1999. Macroscopic seismic anomalies and submarine pockmarks in the Corinth-Patras rift, Greece. Tectonophysics 308, 275-290.

Sultan, N., et al. 2010, Hydrate dissolution as a potential mechanism for pockmark formation in the Niger Delta: J. Geophys. Res. 115, B08101, doi:10.1029/2010JB007453.

Sultan, N., et al. 2011. Dynamics of fault-fluid-hydrate system around a shale-cored anticline in deepwater Nigeria. J. Geophys. Res. 116, B12110, doi:10.1029/2011JB008218.

Sultan, N., et al. 2007a. Potential role of compressional structures in generating submarine slope failures in the Niger Delta. Mar. Geol. 240, 235-255.

Sultan, N., et al. 2007b. Detection of free gas and gas hydrate based on 3D seismic data and cone penetration testing: An example from the Nigerian Continental Slope. Mar. Geol. 240, 235-255.

Sun, Q., et al. 2012. Shallow gas and focused fluid flow systems in the Pearl River Mouth Basin, northern South China Sea. Mar. Geol. 315-318, 1-14 doi:10.1016/j.margeo.2012.05.003.

Talukder, A.R., 2012. Review of submarine cold seep plumbing systems: leakage to seepage and venting. Terra Nova 24, 255-272, doi:10.1111/j.1365-3121.2012.01066.x.

Taylor, M.H., et al. 2000. Trapping and migration of methane associated with the gas hydrate stability zone at the Blake Ridge Diapir: new insights from seismic data. Mar. Geol. 164, 79-89.

Trehu A.M., et al. 2004. Feeding methane vents and gas hydrate deposits at south Hydrate Ridge. Geophys. Res. Lett. 31 (L23310), 1-4, doi:10.1029/2004GL021286.

Trincardi, F., et al. 2004. Evidence of soft-sediment deformation, fluid escape, sediment failure and regional weak layers within the late-Quaternary mud deposits of the Adriatic Sea. Mar. Geol. 213, 91-119.

Ussler III, W., et al. 2003. Submarine pockmarks: a case study from Belfast Bay, Maine. Mar. Geol. 202, 175-192.

Vogt, P.R., et al. 1999. Ground-truthing 11-to 12-kHz side-scan sonar imagery in the Norwegian-Greenland Sea -Part II: Probable diapirs on the Bear Island fan slide valley margins and the Voring Plareau. Geo-Mar. Lett. 19, 111-130.

Wiener, R.W., et al. 2006. Mobile Shale Characteristics and Impact on Structural and Stratigraphic Evolution of the Niger Delta. AAPG/GSTT Hedberg conference, Port of Spain, Trinidad & Tobago.

Waelbroeck, C., et al. 2002. Sea-level and deep water temperature changes derived from benthic foraminifera isotopic records. Quaternary Sci. Rev. 21, 295-305.

Tables

Name	Tool	Length (mbsf)	Water depth (m)	Date deployed (DD/MM/YY)	Observations
CS18	Calypso piston corer	17.76	762	20/05/2008	Silty layer at about 10 mbsf
CS31	Calypso piston corer	10.56	752	06/06/2008	Silty layers at about 6 and 17 mbsf
CPT09S07	CPTu	30	761	10/05/2008	Cone resistance peak at 16 mbsf
CPT09S08	CPTu	30	761	11/05/2008	Cone resistance peak at 19 and 26 mbsf
PZS13	Piezometer 5 sensors	12	761	20/05/2008	Deployment duration: 389 d Depth of sensors (mbsf): P1 - 0.83, P2 - 3.88, P3 - 6.93, P4 - 9.98, P5 - 11.48
PZS14	Piezometer 5 sensors	12	753	20/05/2008	Deployment duration: 412 d Depth of sensors (mbsf): P1 - 0.83, P2 - 3.88, P3 - 6.93 , P4 - 9.98, P5 - 11.48

Table 1: Basic information about Calypso sediment cores, piezocone tests (CPTu) and piezometers.

Figures

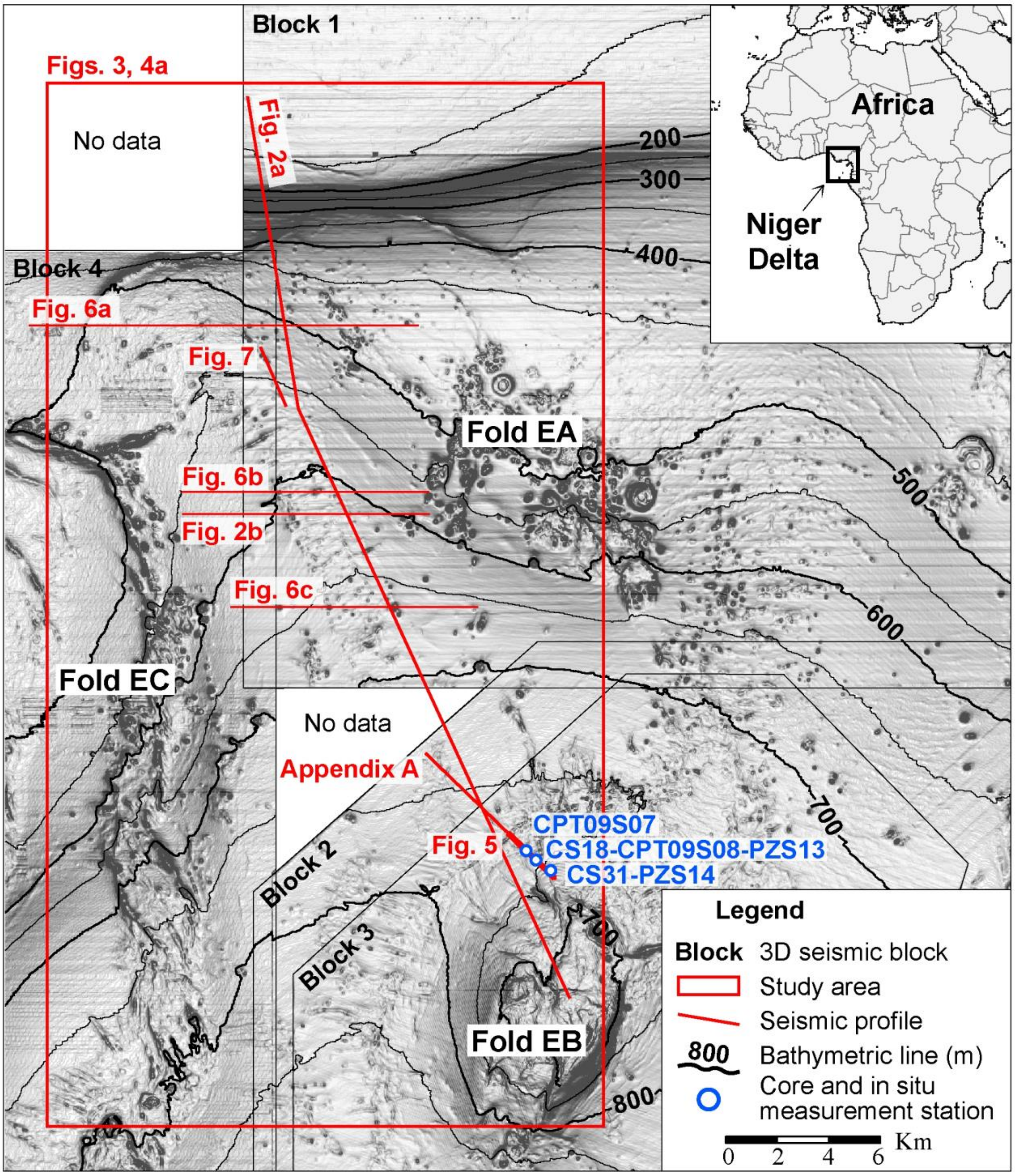

Figure 1: Location map of the Eastern Niger Submarine Delta. The seafloor dip map of the study area with 50-m spaced bathymetric contour has a 25 m horizontal resolution (modified from Riboulot et al., 2012). This map is generated from seismic seabed picking with Sismage software provided by Total. The red lines and boxes are the figure location presented in this paper.

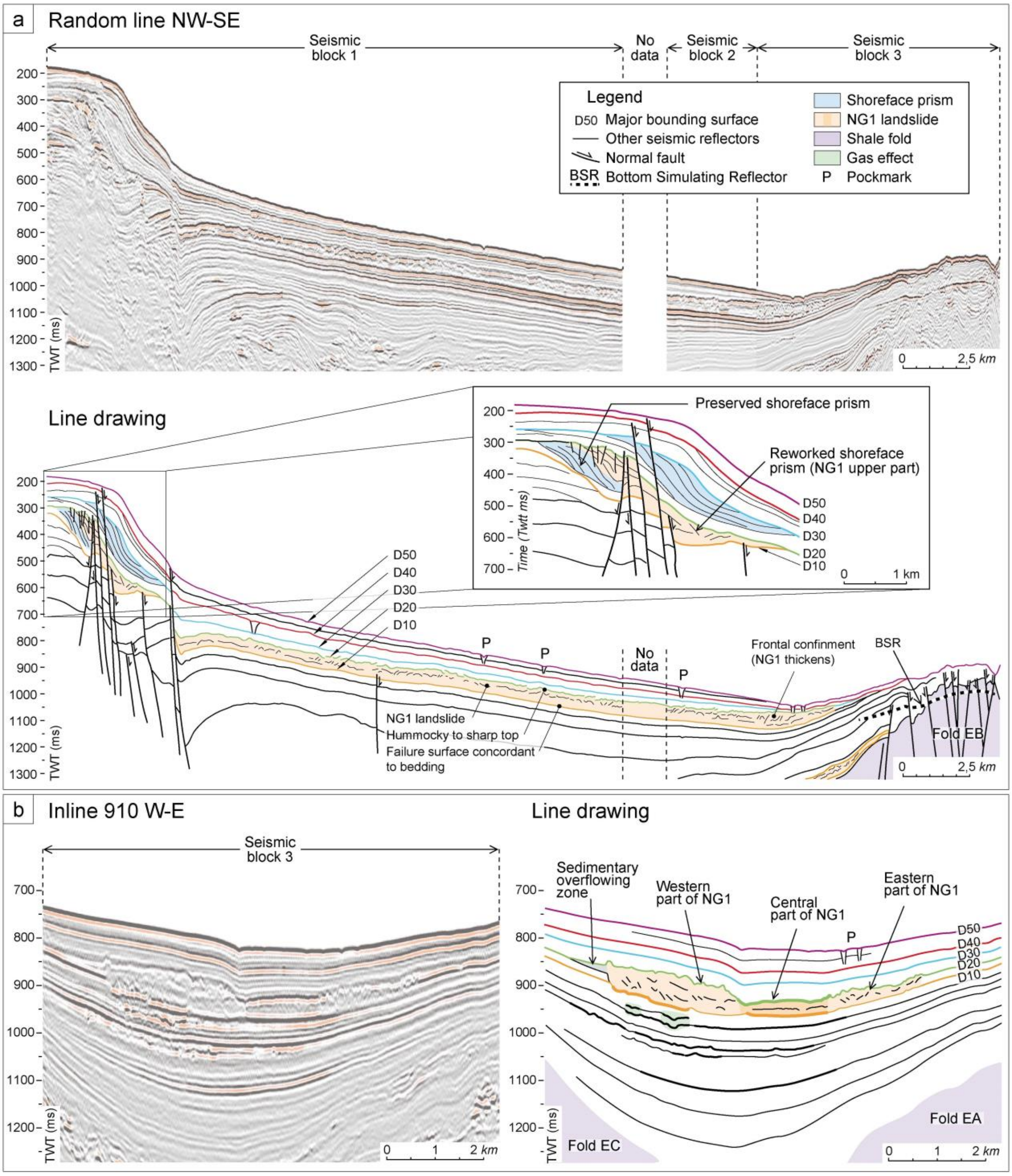

Figure 2: Geometry of the stratigraphic organization of the ENSD with NG1 landslide. a: Uninterpreted regional random line oriented NW-SE, from reprocessed exploration 3D seismic data, showing depositional sequences from the outer continental shelf to the upper continental slope. This line shows the structural organization of the study area (location in Fig. 1). The NG1 landslide affects the outer shelf and finishes on the shale fold EB. The Dxx seismic reflectors represent regional surfaces marking lowstands. The close up view of the outer shelf shows the stacking pattern of shoreface prisms detailed in Riboulot et al., (2012) and the upper part of the NG1 lanslide affecting a shoreface prism. b: Transversal inline 910 oriented W-E, from reprocessed exploration 3D seismic data, showing NG1 with its 3 internal units. The D60 seismic reflector is in blue, and the NG1 landslide in orange.

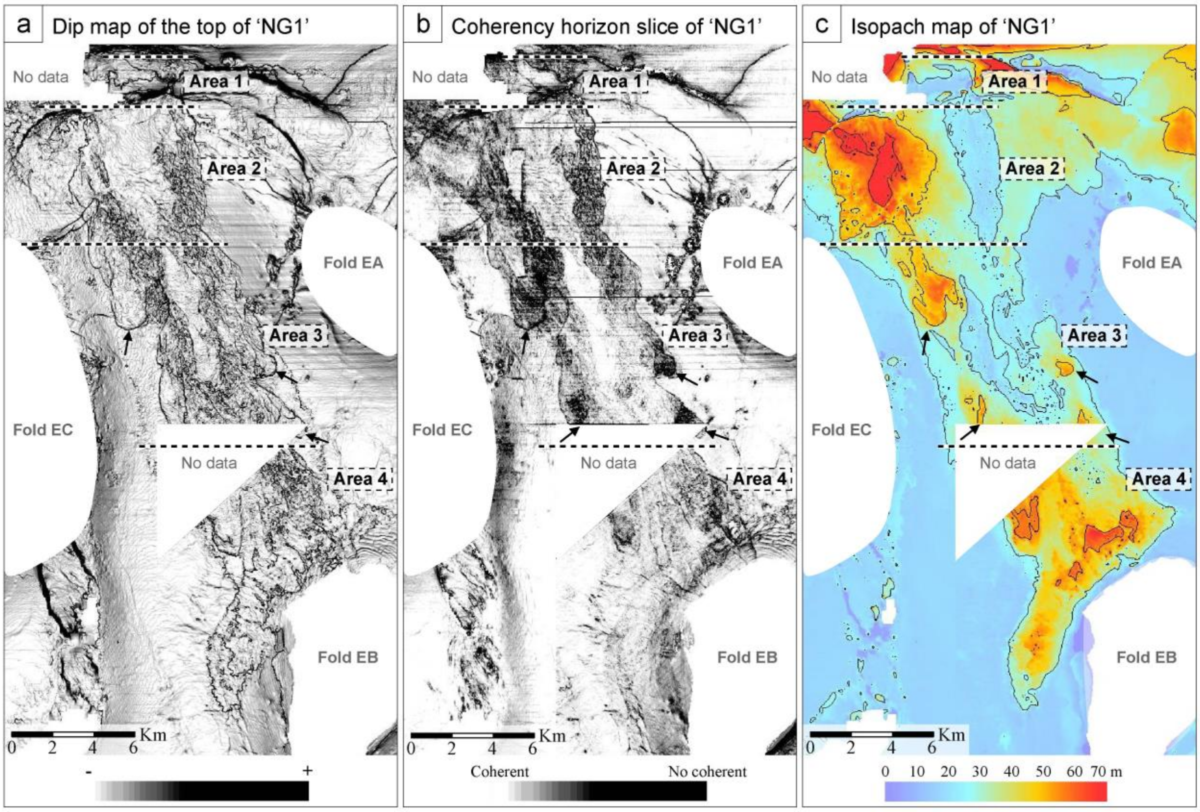

Figure 3: NG1 landslide characteristics illustrated by seismic attribute maps extracted from Sismage software. a: Seismic reflection dip magnitude map of the top of the NG1 landslide. b: Chaotism map exhibiting a variety of forms including the extent of NG1 landslide and the remained character of the internal units of NG1. c: Isopach map of the Top 'NG1' horizon – Base 'NG1' horizon interval, showing the sedimentary accumulation heterogeneities due to the slide (dashed lines separate Areas 1 to 4).

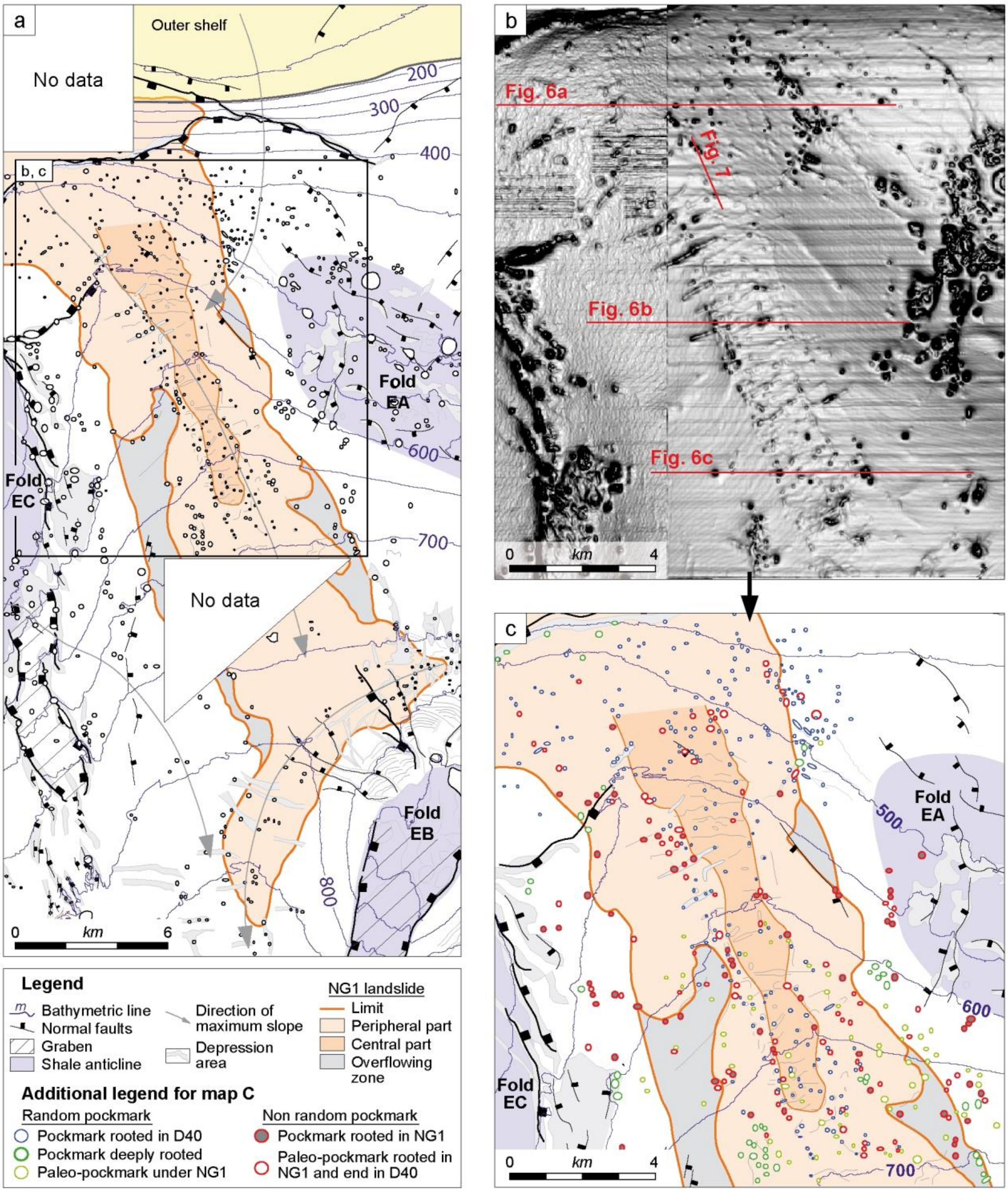

Figure 4: a: Geomorphologic map of NG1 landslide and surrounding area obtained from the interpretation of the bathymetric map and of the 3D seismic data. Faults affecting the seabed are in black, pockmarks in black and white, shale folds in grey and outer continental shelf in yellow. b: Dip map of the study area with location of the following figures in red. c: Geomorphologic map of the study area showing the different group of pockmarks described in the study area from the interpretation of 3D seismic data. The non random pockmarks (in red) are rooted in the NG1 internal discontinuities, while the random pockmarks (in blue) are connected to D40 reflector and the random pockmarks (in green) are more deeply rooted.

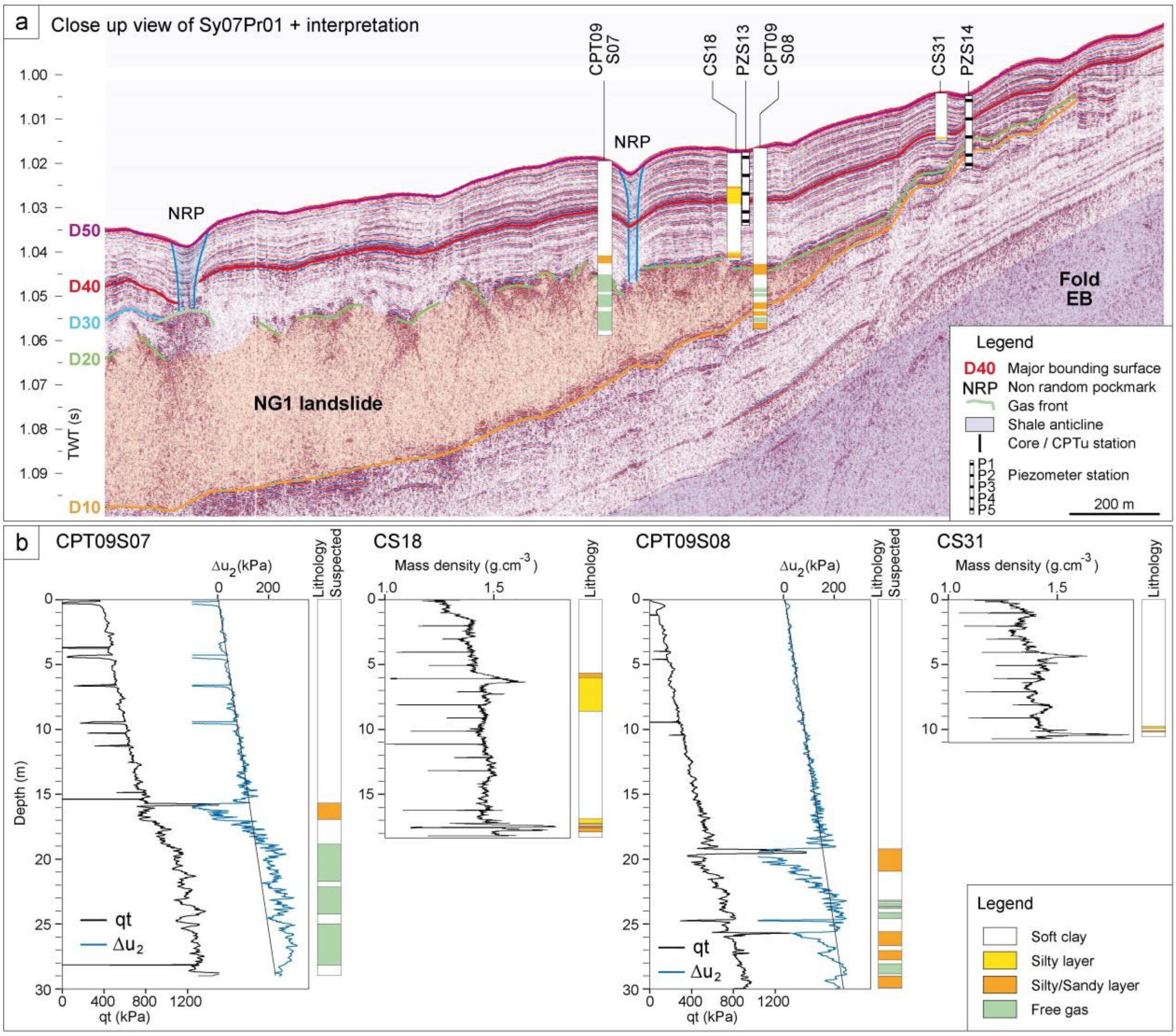

Figure 5: a: Close up view of the 2D HR seismic lines presented in Appendix B with interpreted piezocone and core data. NRP = Non Random Pockmark. b: Corrected cone resistance qt and excess pore pressure Δu2 versus depth from sites CPT09S07 and CPT09S08. Mass density values versus depth and lithology presented for cores CS18 and CS31. See text for details.

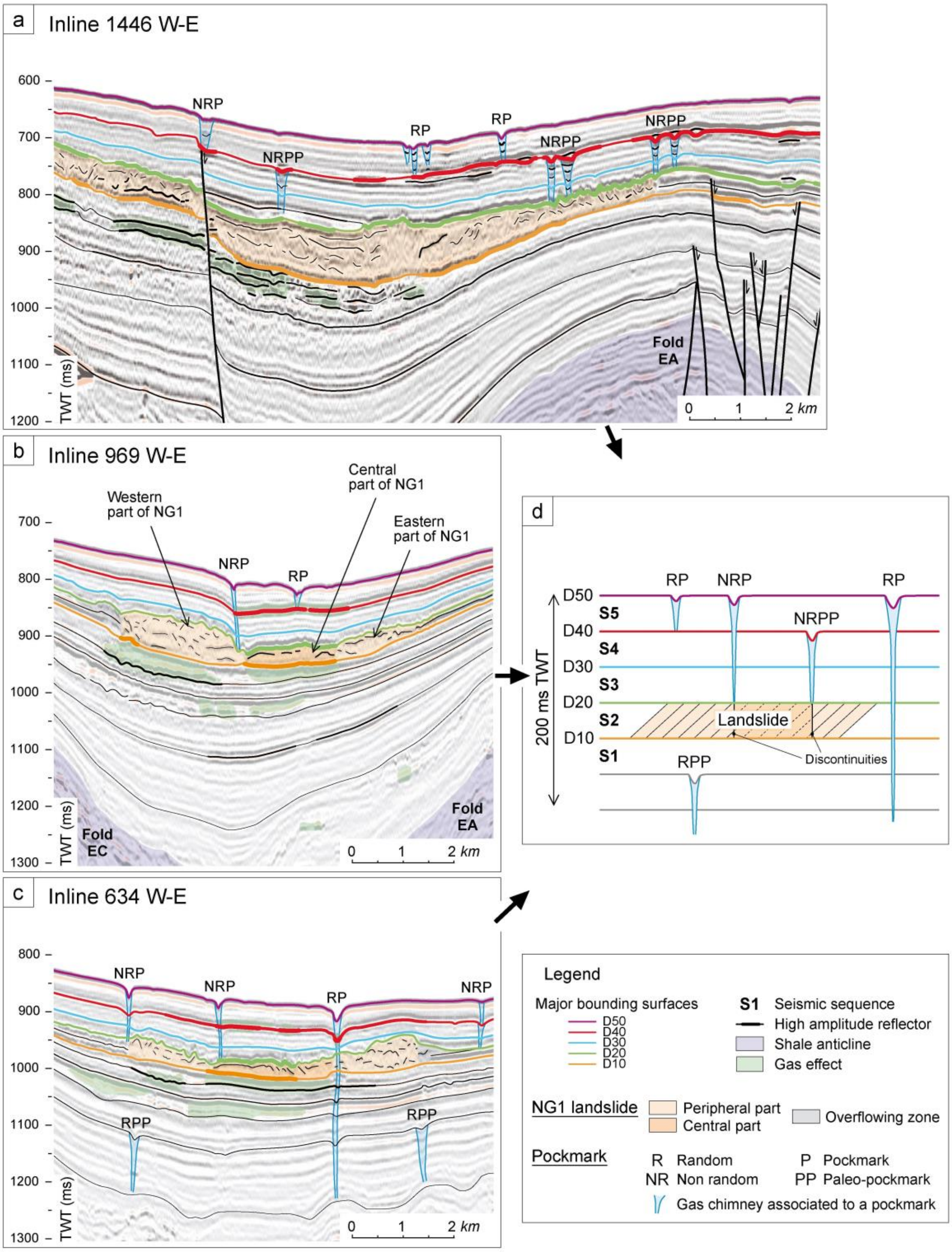

Figure 6: a: Seismic transversal inline 1446 oriented W-E, from reprocessed exploration 3D seismic data, with its seismic interpretation showing: (1) non random pockmarks connected with NG1 landslide ending up in D40 reflector, and (2) random pockmarks rooted in the D40 reflector. b: Seismic transversal inline 969 oriented W-E, from reprocessed exploration 3D seismic data, with its seismic interpretation showing: (1) non random pockmarks rooted in NG1 landslide internal discontinuities, and (2) pockmarks rooted in the D40 reflector. c: Seismic transversal inline 634 oriented W-E, from reprocessed exploration 3D seismic data, with its seismic interpretation showing: (1) non random pockmarks rooted in NG1 landslide internal discontinuities, (2) random paleo-pockmarks, and (3) random pockmarks deeply rooted. d: Summary of organization of the stratigraphic pattern and location of all types of pockmarks observed in the study area. See text for details.

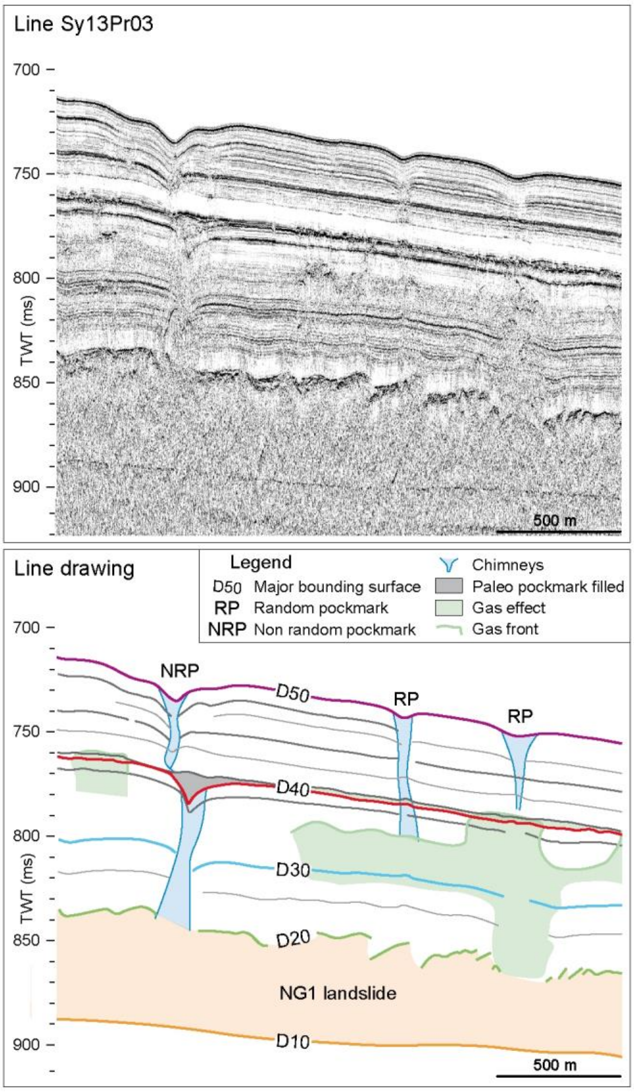

Figure 7: 2D HR seismic lines acquired with the SYSIF system along the same track of the seismic line presented in Figure 2, showing more details about the features described and the precise location of fluids within sediment.

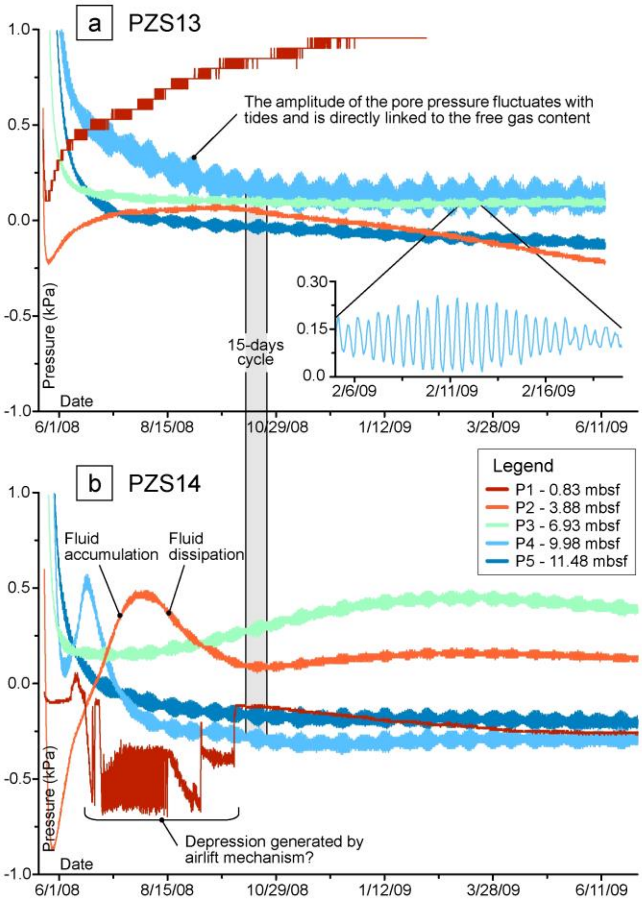

Figure 8: a: Excess pore water pressure of the 5 sensors (P1 to P5) of PZS13, b: excess pore water pressure of the 5 sensors (P1 to P5) of PZS14, and c: excess pore water pressure of 2 sensors (P1 and P2) of PZS14. See text for details.

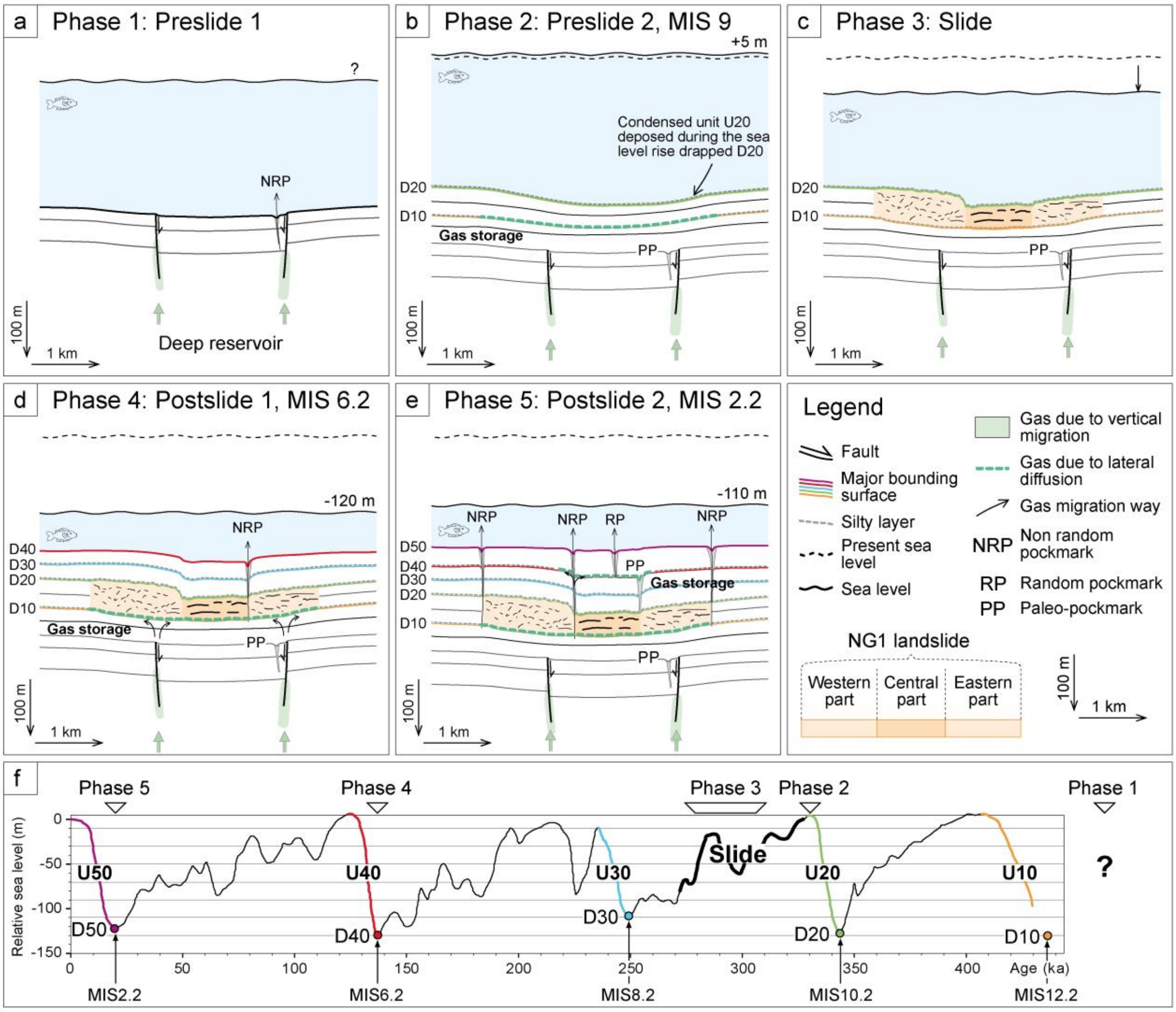

Figure 9: Conceptual model (Idealized scenario) of development of pockmark field controlled by fluid seepages throughout a landslide. The scenario, valid for the observations made in this paper, is composed of 5 phases (a, b, c, d, e) detailed in the discussion. f: Sea-level change curve (Waelbroeck et al., 2002) indicates the timing of phases 1 to 5 of pockmarks and landslide formation.

Supplementary material

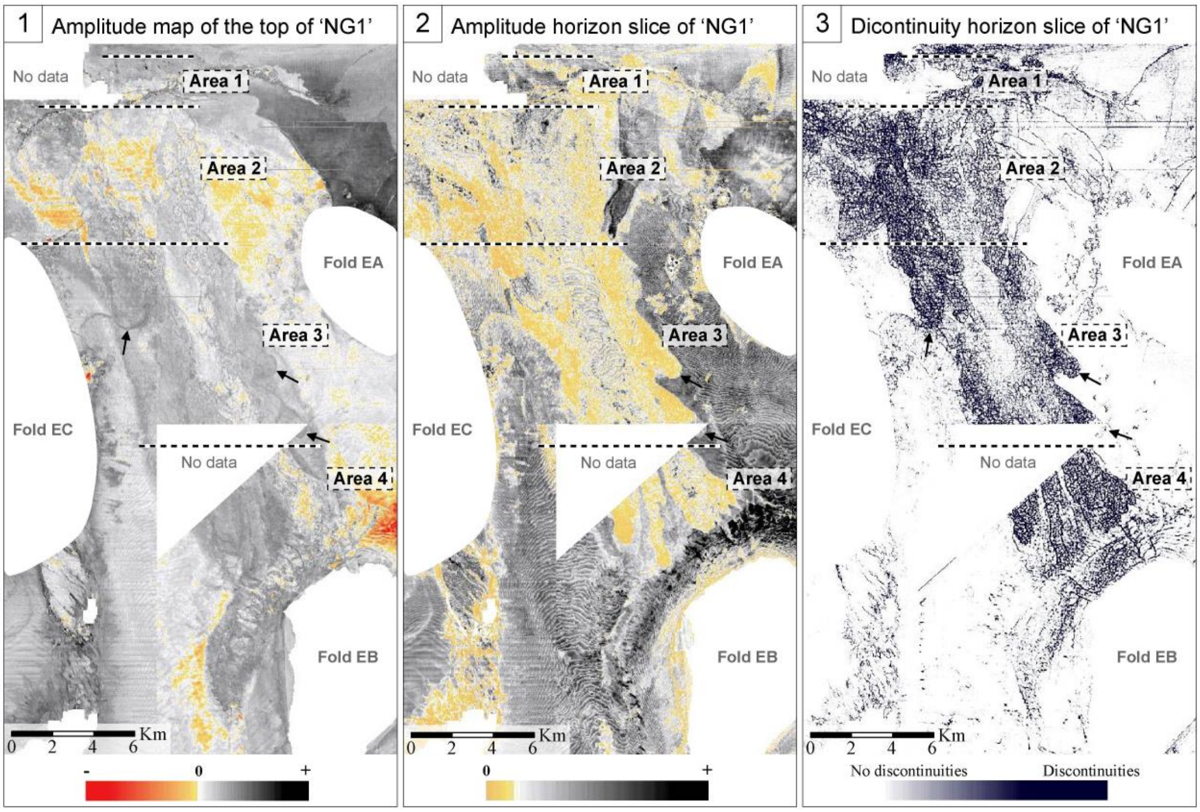

Appendix A: NG1 landslide characteristics illustrated by seismic attribute maps extracted from Sismage software. 1: Seismic reflection amplitude map of the top of the NG1 landslide. 2: Amplitude map showing the stratification of the central unit and the reworked character of the western and the eastern units. 3: Fault map showing faults, pockmarks and the discontinuities within NG1 (dashed lines separate Areas 1 to 4).

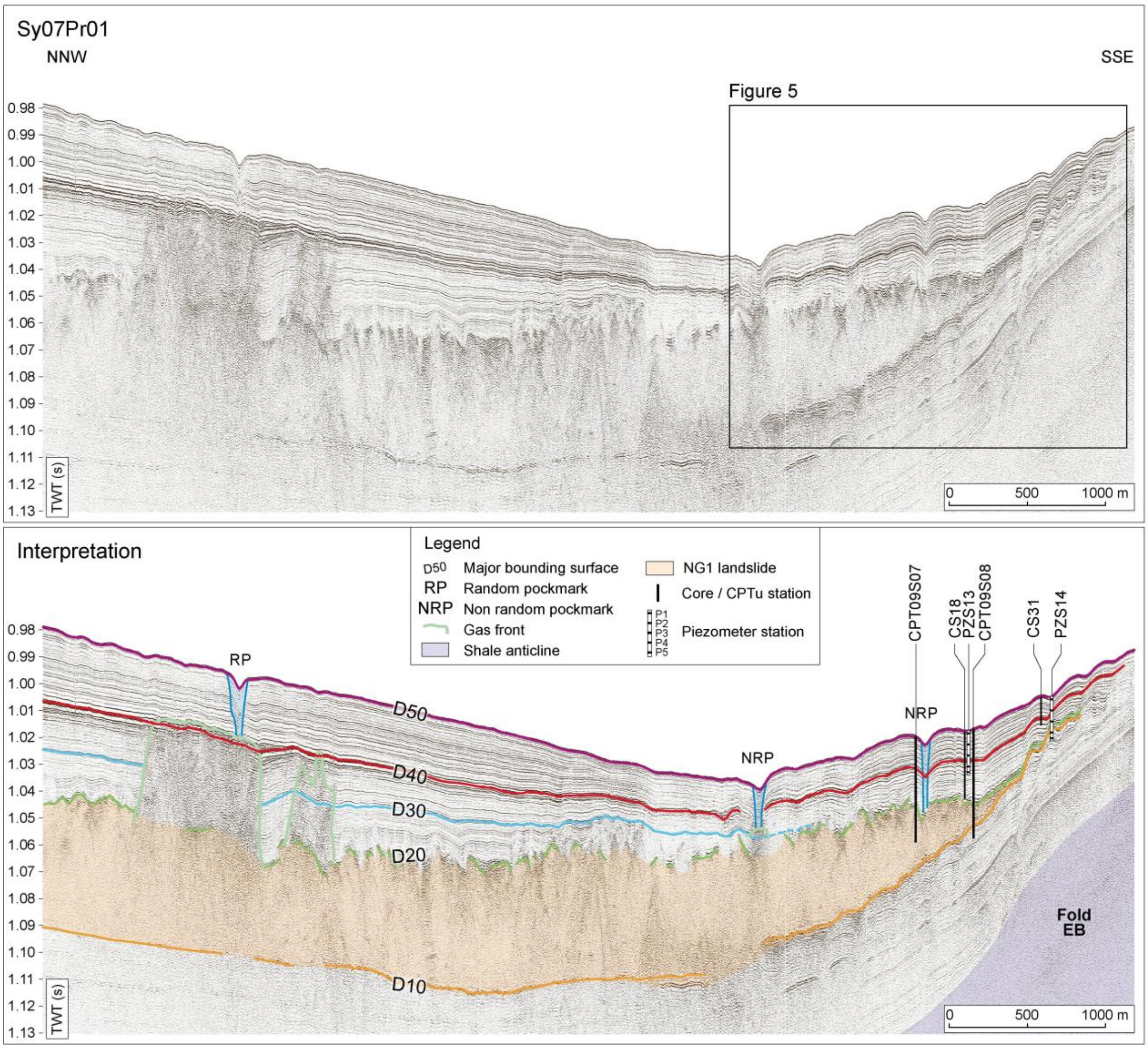

Appendix B: 2D HR seismic lines acquired with the SYSIF system along the same track of the seismic line presented in Figure 5 with location of piezocone and core stations. The high amplitude reflectors named Dxx are interpreted as coarse grain layers from coring and *in situ* measurements. D20 reflector on top of NG1 is discontinuous with local deformation and disruption.